32ND INTERNATIONAL COSMIC RAY CONFERENCE, BEIJING 2011

Strong New Constraints on the Extragalactic Background Light in the Near- to Mid-Infrared

M. ORR[1], F. KRENNRICH[1], E. DWEK[2]
[1]*Department of Physics and Astronomy, Iowa State University, Ames, IA 50011*
[2]*Observational Cosmology Lab, Code 665, NASA Goddard Space Flight Center, Greenbelt, MD 20771*
morr@iastate.edu
DOI: 10.7529/ICRC2011/V08/0960

Abstract: The extragalactic background light (EBL) is comprised of all nuclear and gravitational energy releases since the epoch of recombination. Its intensity is surpassed only by that of the cosmic microwave background. Very high energy (VHE) gamma-rays from blazars, as they propagate through the Universe, interact via pair production with the photons comprising the EBL. Signatures of EBL absorption are therefore imprinted on the observed spectra of blazars. Current generation imaging atmospheric Cherenkov telescopes (IACTs), operating at energies from ~ 100 GeV to ~ 30 TeV, can probe the emission spectra of blazars for clear signatures of EBL absorption and place constraints on both the overall intensity and shape of the EBL spectral energy distribution. In this talk we will discuss our recent work to constrain the EBL utilizing two distinct analysis techniques applied to the high energy spectra of blazars.

Keywords: blazars, extragalactic background light, gamma rays, infrared diffuse background

1 Introduction

The extragalactic background light (EBL) contains all radiative energy releases, from nuclear and accretion processes, that have occurred since the epoch of recombination. Its spectrum is bimodal with peaks at $\sim 1\,\mu$m and $\sim 100\,\mu$m. The optical/infrared (IR) component is produced by the formation of heavy elements and gravitational energy releases and the far-IR component results from the absorption and re-radiation by dust of this emission. The energy spectrum contains, therefore, important information about the cosmic evolution of these energy sources, the obscuring dust, and the relative contributions of starburst galaxies and AGNs to the energy released over cosmic time.

Very-high-energy (VHE) gamma rays ($\sim 0.1-10$ TeV) interact, via pair production, with photons in the near- to mid-IR regime of the EBL (i.e., $\gamma_{\rm VHE}\,\gamma_{\rm EBL} \rightarrow {\rm e}^+\,{\rm e}^-$) [1]. Due to the energy dependence of the $\gamma-\gamma$ optical depth, the observed VHE emission spectra of blazars are softer than the intrinsic spectra. Information regarding the EBL spectral energy distribution (SED) can be gleaned from this spectral absorption using a variety of approaches [2, 3, 5]. In this paper, we present two different approaches to constrain the EBL, described in the sections entitled Method 1 and Method 2. A more detailed discussion of this work can be found in [6].

2 EBL Models Tested

The EBL models tested here were derived from what will be referred to throughout the text as the baseline model. This baseline model follows the shape outlined by lower limits derived from galaxy counts obtained with the Hubble Space Telescope [7, 8], the Spitzer Space Telescope [9, 10], and the Infrared Space Observatory [11]. An approach similar to that of [12], using third order splines, was implemented to produce this baseline EBL model.

Since the absorption of TeV gamma-rays by EBL photons is sensitive to the intensity at near- and mid-IR wavelengths, the regions between $\sim 0.3-7\,\mu$m and $\sim 7-50\,\mu$m were independently scaled to explore a variety of EBL shapes. The left panel of Figure 1 illustrates the range of scenarios investigated (shaded region). The right panel of Figure 1 shows the calculated gamma-ray optical depths given each EBL scenario. All optical depths were calculated assuming the cosmological parameters $H_0 = 70\,{\rm km\,s^{-1}\,Mpc^{-1}}$, $\Omega_m = 0.3$, and $\Omega_\Lambda = 0.7$.

2.1 Method 1

The first method implemented to constrain the intensity of the EBL used blazar spectra measured by the *Fermi* Large Area Telescope (LAT; Atwood et al. 2009) as a proxy for their intrinsic spectra in the TeV regime. Measurements made by imaging atmospheric Cherenkov telescopes (IACTs) were used to calculate a de-absorbed spectrum for each EBL model discussed above. This technique was

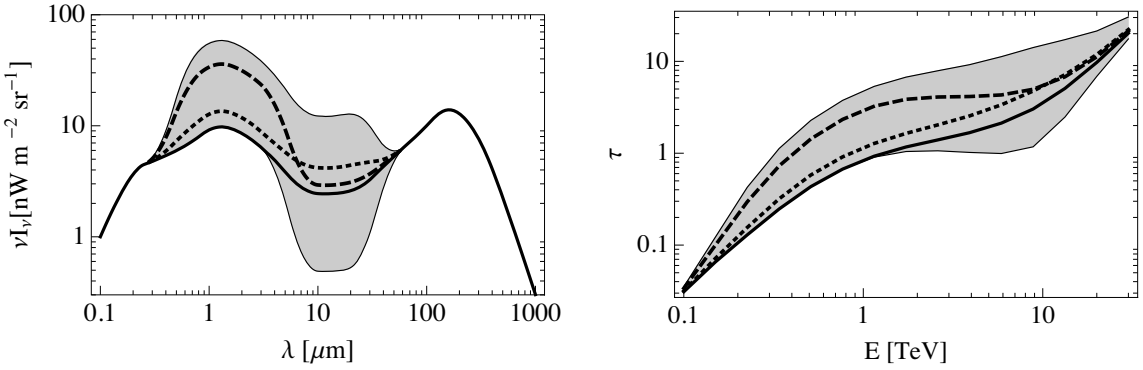

Figure 1: *Left*: EBL intensity versus photon wavelength. The shaded region indicates the range of scenarios tested. The thick solid line designates the baseline shape used, from which all other scaled shapes are generated. For clarity, two additional models are shown (dotted and dashed) illustrating the independent scaling of the near- and mid-IR regions. *Right*: Optical depth τ (at $z = 0.1$) versus gamma-ray energy in TeV for each EBL scenario tested. The optical depths for the baseline and two additional EBL models shown in the left panel are shown as well.

applied to the four hard-spectrum blazars 1ES 0229+200, RGB J0710+591, 1ES 1101-232, and 1ES 1218+304 (see Table 1).

The intrinsic TeV source spectra were determined following the relationship

$$\left(\frac{\mathrm{d}N}{\mathrm{d}E}\right)_{\mathrm{intr}} = \left(\frac{\mathrm{d}N}{\mathrm{d}E}\right)_{\mathrm{obs}} e^{\tau(E,z)}, \qquad (1)$$

where $(\mathrm{d}N/\mathrm{d}E)_{\mathrm{intr}}$ is the intrinsic spectrum, $(\mathrm{d}N/\mathrm{d}E)_{\mathrm{obs}}$ is the observed spectrum, and $\tau(E, z)$ is the gamma-ray optical depth at energy E and source redshift z. The intrinsic spectrum was assumed to have a power-law form given by

$$\left(\frac{\mathrm{d}N}{\mathrm{d}E}\right)_{\mathrm{intr}} = N_0 \left(\frac{E}{E_0}\right)^{-\Gamma}, \qquad (2)$$

where N_0 is the normalization at energy E_0, E is the energy, and Γ is the spectral index. The condition used to evaluate the consistency between the intrinsic TeV spectrum and the extrapolated *Fermi* spectrum was given by

$$|\Gamma_{\mathrm{TeV}} - \Gamma_{\mathrm{GeV}}| \leq N\sqrt{\sigma^2_{\mathrm{TeV}} + \sigma^2_{\mathrm{GeV}}}, \qquad (3)$$

where Γ_{TeV} and σ^2_{TeV} are the calculated IACT *intrinsic* spectral index and variance, respectively, Γ_{GeV} and σ^2_{GeV} are the *Fermi* spectral index and variance, respectively, and N is the confidence level in units of standard deviations. An EBL scenario was considered viable if the de-absorbed spectrum satisfied the set criteria for consistency with the intrinsic spectrum predicted by the *Fermi* extrapolation. This criterion was that Γ_{TeV} be within $\pm N\sigma$ of Γ_{GeV} (i.e., Equation 3), where N was 1, 2, or 3.

2.2 Method 2

The interaction of gamma rays with EBL photons can produce absorption signatures in the observed spectra of blazars. This signature, which manifests as a spectral break, is produced by changes in the slope of the γ-γ optical depth. As illustrated in the right panel of Figure 1, the optical depth calculated for certain EBL scenarios is nearly flat in the energy range of $\sim$1 $-$ several TeV resulting in an approximately energy independent absorption of gamma-rays. The observed spectral index in this energy range will be closer to the intrinsic value – producing a break in the spectrum at $\sim$1 TeV. The magnitude of this break increases with the source redshift and depends on the near- to mid-IR ratio [13]. With currently available data, no individual blazar spectrum is likely to show a statistically significant break in its spectrum. However, a large sample of blazars may reveal a redshift dependent trend. The presence/absence of such a trend in observations can be used to constrain the EBL. Table 1 lists the sample of blazars used to perform this study.

The shape of the EBL uniquely determines the spectral break versus redshift distribution and was calculated here for a multitude of scenarios using a test blazar spectrum. This test spectrum was chosen to represent the "average" spectrum of the blazars listed in Table 1. To generate this spectrum, the average lowest energy bin, highest energy bin, and number of bins in the sample were calculated. This resulted in a test spectrum characterized by 8 energy bins ranging from 200 GeV to 5 TeV. The Crab Nebula flux at 1 TeV was used for the spectral normalization along with an intrinsic spectral index of 1.5. The underlying assumption in this method is that the intrinsic blazar spectrum is well described by a single power-law (of arbitrary index) over the energy range considered.

The absorbed spectra were calculated using the inverse relation of Equation 1. Each spectrum was fit with a broken power-law normalized to the best-fit flux at the assumed break energy of 1.3 TeV (the choice of which is motivated by the near-IR peak at $\sim$1 μm in the EBL scenarios used

Table 1: Blazar sample used in the described analyses. The columns are as follows (left to right): source name, source redshift, GeV and TeV spectral indices, analysis technique performed with the source spectrum, reference to the TeV spectrum, number of TeV spectral points less than (l.t.) and greater than (g.t.) 1.3 TeV, and the measured spectral break at 1.3 TeV. All errors given are statistical only. See Orr et al. (2011) [6] for a list of references to the TeV spectra used. Unless otherwise indicated, $\Gamma_{\rm GeV}$ is taken from the *Fermi* 1 Year Catalog (`http://fermi.gsfc.nasa.gov/ssc/data/access/lat/1yr_catalog/`).

Source Name	Redshift	Spectral Index		Method	# Spec. Points	$\Delta\Gamma$
		$\Gamma_{\rm GeV}$	$\Gamma_{\rm TeV}$	Used		l.t./g.t. 1.3 TeV
1ES 2344+514	0.044	1.57 ± 0.17	2.95 ± 0.12	2	4/3	-0.39 ± 1.11
1ES 1959+650	0.048	2.10 ± 0.05	2.58 ± 0.18	2	4/2	-0.61 ± 1.01
PKS 0548-322	0.069	-	2.8 ± 0.3	2	3/2	1.75 ± 0.83
PKS 2005-489	0.071	1.90 ± 0.06	4.0 ± 0.4	2	6/3	1.93 ± 2.30
RGB J0152+017	0.080	-	2.95 ± 0.36	2	4/2	0.96 ± 1.18
PKS 2155-304†	0.117	1.91 ± 0.02	3.32 ± 0.06	2	7/3	0.30 ± 0.40
RGB J0710+591	0.125	1.30 ± 0.16*	2.69 ± 0.26	1,2	3/2	-0.96 ± 1.14
H 1426+428	0.129	1.49 ± 0.18	3.50 ± 0.35	2	3/4	2.11 ± 0.55
1ES 0229+200	0.140	1.50 ± 0.20*‡	2.50 ± 0.19	1,2	3/5	0.39 ± 0.62
1ES 1218+304	0.182	1.69 ± 0.07*	3.07 ± 0.09	1,2	7/2	1.33 ± 1.35
1ES 1101-232	0.186	1.61 ± 0.26*	2.88 ± 0.17	1,2	9/4	1.64 ± 0.64
1ES 0347-121	0.188	-	3.10 ± 0.23	2	4/3	1.28 ± 0.89

* *Fermi* analysis performed in this work.
† $<1\%$ probability of being a steady *Fermi* source.
‡ *Fermi* has a weak detection of 1ES 0229+200 at $\sim 4\sigma$. For this analysis we have *assumed* a *Fermi* spectral index of 1.5 ± 0.2.

here). The spectral break was defined as

$$\Delta\Gamma = \Gamma_1 - \Gamma_2, \tag{4}$$

where Γ_1 and Γ_2 are the spectral indices below and above $E_{\rm break}$, respectively. With this definition, a spectral hardening above the break energy would result in a positive $\Delta\Gamma$. From here the distribution of $\Delta\Gamma$ as a function of redshift was determined for each EBL scenario. This process was repeated 100 times, mimicking multiple independent observations, each time yielding a different result due to Gaussian fluctuations introduced into the spectra. This facilitated the determination of the break versus redshift distribution to an arbitrary precision and accuracy.

Each distribution was fit with a line, i.e.,

$$\Delta\Gamma(z) = m\,z + b\,, \tag{5}$$

where $\Delta\Gamma(z)$ is the spectral break at redshift z and m and b are free parameters. Using the best linear fit obtained from observational data, the 1σ, 2σ, and 3σ two dimensional contours in slope and intercept space (i.e., m and b, respectively, in Equation 5) were determined. The best fit results from the expected spectral break versus redshift distribution for each EBL scenario were then compared with the observationally derived contours. If the fit parameters for a particular scenario fell within the two dimensional 1σ contour, this scenario was included as part of the 1σ contour in EBL parameter space. The 2σ and 3σ contours in EBL parameter space were determined in the same fashion.

To determine the spectral break versus redshift distribution ($\Delta\Gamma(z)$), a sample of 12 blazars (Table 1) with spectra extending both above and below the break energy were fit with a broken power-law. Figure 2 shows the distribution of $\Delta\Gamma(z)$ versus the source redshift for all blazars in the sample. Two linear fits were performed on the data – one leaving the intercept $\Delta\Gamma(0)$ as a free parameter and one with the intercept fixed to 0. The results of these two fits were

$$\Delta\Gamma(z) = \begin{cases} (8.68 \pm 5.37)z - (0.24 \pm 0.71), \\ \qquad\qquad \chi^2/\nu = 14.10/10 \\ (6.95 \pm 1.65)z, \\ \qquad\qquad \chi^2/\nu = 14.22/11 \end{cases} . \tag{6}$$

In the absence of any spectral break one would expect $\Delta\Gamma(z) = 0$. The data exclude this hypothesis at the $\sim 3.2\sigma$ level.

3 Combining Methods 1 & 2

The EBL constraints obtained with Method 1 are determined by the overall hardness/softness of the calculated intrinsic TeV spectra for each EBL scenario. This makes this technique sensitive to the overall intensity of the EBL. Method 2 relies on a relative measurement, i.e., the presence of a spectral break at 1.3 TeV. Consequently, this technique is predominantly sensitive to the ratio of intensities between the near- and mid-IR wavelength regimes.

Given their complementarity, Improved constraints on the EBL can be obtained by combining the results from Methods 1 and 2. Figure 3 shows the 2σ confidence region for the EBL SED derived from the combination of these analyses.

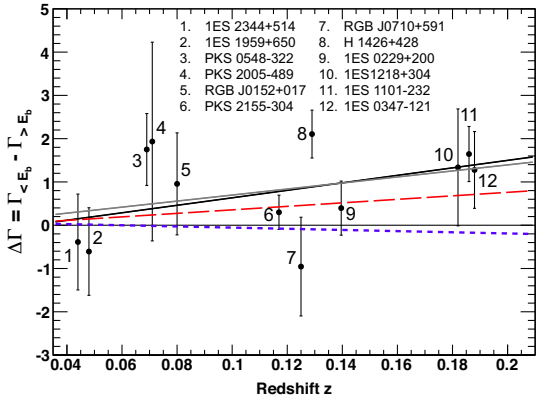

Figure 2: Distribution of the observed spectral break versus redshift for the sample of 12 blazars (see Table 1). The spectral break is defined as the spectral index below the break energy $E_{\rm b}$ minus the spectral index above the break energy. The black (grey) solid line represents the best linear fit leaving the y-intercept free (fixed to zero). The fit results are given in Equation 6. The long- and short-dashed lines show the $\Delta\Gamma(z)$ distributions expected from the scenario of Aharonian et al. (2006) [2], scaled by a factor of 0.55, and the model of Franceschini et al. (2008) [16], respectively.

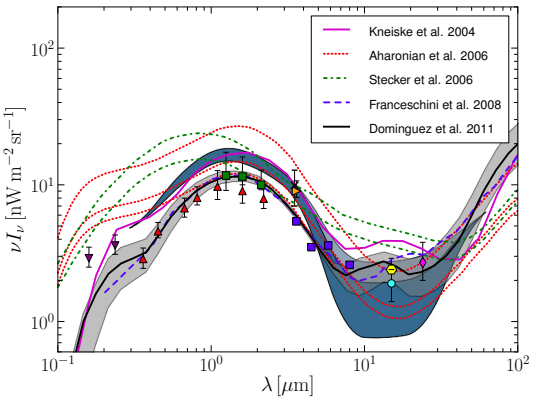

Figure 3: Approximate EBL SED 2σ confidence region (blue shaded area) derived from Methods 1 and 2. Also shown are the models of: Aharonian et al. (2006) [2] (dotted lines) scaled by 1.0, 0.55, and 0.45; Stecker et al. (2006) [15] (dot-dashed lines) fast evolution (upper) and baseline (lower) models; Franceschini et al. (2008) [16] (dashed line); Kneiske et al. (2004) [14] (upper solid line); Domínguez et al. (2011) [17] (lower solid line and grey shaded area). The filled symbols represent galaxy count lower limits (see Orr et al. (2011) [6] for a complete list of references). The $\times$ at 3.5 μm indicates the tentative detection of Dwek & Arendt (1998) [18].

4 Discussion & Conclusions

We have presented constraints on the EBL intensity using two distinct methods for the analysis of blazar spectra. Method 1 primarily constrains the overall EBL intensity, whereas Method 2 primarily constrains the relative EBL intensities in the near- and mid- IR. The two approaches are therefore complementary and provide a closed confidence range for the EBL intensity. This is the first time these methods have been used to derive such a contour for the EBL SED.

Our analysis has shown the advantages of using these two complementary approaches in constraining the EBL. Our EBL constraints are consistent with some models from other authors, such as the scaled version of Aharonian et al. (2006) [2]. However, the models of Stecker et al. (2006) [15], Franceschini et al. (2008) [16], Kneiske et al. (2004) [14], and Dominguez et al. (2011) [17] are disfavored by our analysis at $> 3\sigma$ confidence level. It has also provided evidence that the near- to mid-IR ratio of the EBL may be larger than previously thought. Future measurements with Fermi, as well as both current and next generation IACTs, such as the Cherenkov Telescope Array (CTA), will continue to improve these constraints.

Acknowledgements

FK acknowledges support from DOE. ED and FK acknowledge support from the *Fermi* Cycle-2 Guest Investigator program.

References

[1] Gould, R. J., & Schréder, G. P. 1967, Phys. Rev., 155, 1408
[2] Aharonian, F., et al. 2006, A&A, 448, L19
[3] Aharonian, F., et al. 2007, A&A, 475, L9
[4] Acciari, V. A., et al. 2010, ApJ, 709, L163
[5] Dwek, E., & Krennrich, F. 2005, ApJ, 618, 657
[6] Orr, M., Krennrich, F., & Dwek, E. 2011, ApJ, 733, 77
[7] Gardner, J. P., Brown, T. M., & Ferguson, H. C. 2000, ApJ, 542, L79
[8] Madau, P., & Pozzetti, L. 2000, MNRAS, 312, L9
[9] Fazio, G. G., et al. 2004, ApJS, 154, 39
[10] Papovich, C., et al. 2004, ApJS, 154, 70
[11] Elbaz, D., et al. 2002, A&A, 384, 848
[12] Mazin, D., & Raue, M. 2007, A&A, 471, 439
[13] Imran, A., & Krennrich, F. 2008, Proc. 30th ICRC, 3, 981
[14] Kneiske, T. M., Bretz, T., Mannheim, K., & Hartmann, D. H. 2004, A&A, 413, 807
[15] Stecker, F., Malkan, M., & Scully, S. 2006, ApJ, 648, 774
[16] Franceschini, A., Rodighiero, G., & Vaccari, M. 2008, A&A, 487, 837
[17] Domínguez, A., et al. 2011, MNRAS, 410, 2556
[18] Dwek, E., & Arendt, R. G. 1998, ApJ, 508, L9